Received July 29, 2017, accepted August 14, 2017, date of publication August 21, 2017, date of current version September 19, 2017.

Digital Object Identifier 10.1109/ACCESS.2017.2740955

Reproduction Methodology for Single Phase-to-Ground Faults in Overhead Transmission Lines

HANQING LIANG, YADONG LIU, (Member, IEEE), GEHAO SHENG, (Member, IEEE), AND XIUCHEN JIANG

Department of Electrical Engineering, Shanghai Jiaotong University, Shanghai 200240, China

Corresponding author: Hanqing Liang (lianghanedu2016@163.com)

This work was supported in part by the National Natural Science Foundation of China under Grant 51307109 and in part by the Science and Technology Project of State Grid Corporation in China.

ABSTRACT Reproducing key fault information quantitatively has practical significance for the fault diagnosis of overhead transmission lines (OLTs). In order to reproduce the key fault information of a single phase-to-ground (SPG) fault, this paper proposes a reproduction methodology based on the waveform inversion theory and the propagation characteristics of a traveling wave. Based on the frequency-dependent parameter model and the inversion technique, the current traveling wave at the fault point can be obtained. The fault reproduction model was then created based on the wave propagation characteristics and the obtained waveforms at the fault point. The proposed method adopted a chaos particle swarm optimization algorithm to realize a fast search of the solution space, and this contributes to accurately reproducing the fault angle and the fault resistance of a SPG fault. The simulation results demonstrate that the method proves suitable for reproducing the key information at the fault point. In addition, the proposed method was implemented in 500-kV OTLs, which could help to provide data support for fault diagnosis and insulation protection.

INDEX TERMS Fault reproduction, inversion, current traveling wave, fault information, CPSO, fault resistance, fault angle.

I. INTRODUCTION

Overhead transmission lines (OTLs) are susceptible to harsh weather conditions and are considered prone to failures in power systems [1]–[3]. Since OTLs are not able to avoid the effects of adverse climatic conditions actively, the operational reliability of OTLs can only be enhanced by increasing their defensive capacity.

The fault traveling wave of OTLs contains abundant useful fault information [4]–[8], including polarity, arrival time, fault resistance, fault angle, amplitude, and half-wavelength. Several extant studies examined fault location and line protection for OTLs based on the information contained in the traveling wave [4], [9], [10]. Current studies mainly utilize the polarity and the arrival time of a traveling wave to detect the fault section and location. With respect to the detection of the fault traveling wave, the main method involves installing detection devices at substations or OTLs. ''Reproduce'' means to restore the fault information that is difficult to be directly detected. If the traveling wave at the fault point can be obtained, more key fault information (including the amplitude and fault resistance at the fault point) is able to be reproduced. Given this information, it is possible to perform a more effective identification of fault cause as well to inform a better design of OTL insulation. The study in [11] indicated that the reproduced half-wavelength and amplitude of the traveling wave at the fault point contribute to provide higher recognition for the lightning-strike-type faults. However, the traveling wave at the fault point is difficult to obtain due to nonlinear attenuation and distortion that occurs during the propagation of traveling waves.

In order to reproduce the key fault information contained in the traveling wave, it is necessary to adopt specific mathematical methods to first obtain the transient waveform at the fault point. Although this area is new, several methods have been proposed to obtain the waveforms at the fault point and to

reproduce the key fault information. In [12], a novel method was proposed to obtain the waveform at the fault point and reproduce the fault information of a lightning-induced fault based on a lightning current monitoring system and the Cramer rule. The reproduced fault information (rise time, amplitude, and half-wavelength) from the waveforms provide important data support for the insulation design of OTLs. Shu *et al*. [13] provided a deconvolution method to obtain the current waveform at the lightning-strike point and to reproduce the fault information including the amplitude and steepness of the lightning current. The method utilized the transient voltage obtained by a high-speed sampling system installed on OTLs.

The single phase-to-ground (SPG) fault is considered one of the most common faults in OTLs. The transient fault information of a SPG fault, including the fault resistance and fault angle, provides important data support for fault diagnosis as well as for designing insulation protection on OTLs. However, there are few related studies that focus on reproducing the key fault information of a SPG fault. In this study, a reproduction method for a SPG fault was proposed that uses inversion theory and the propagation characteristics of a traveling wave. First, the generating mechanism of the SPG fault traveling wave was analyzed. Then, the frequency-dependent parametric OTL model was created based on inversion theory, and it contributed to obtaining the transient traveling wave at the fault point. Subsequently, the fault reproduction model was built by analyzing the mathematical relationship between the first and second wavefronts obtained from different detection points on OLTs. In addition, the mathematical relationship between the aerial-mode current amplitude, fault angle, and fault resistance at the fault point was obtained based on the principle of wave propagation. Furthermore, a chaos particle swarm optimization (CPSO) algorithm was adopted to solve the objective function of the proposed fault reproduction model, which could help to accurately reproduce the key fault transient information of a SPG fault.

The distributed fault location system of OTLs has undergone considerable development in recent years. In this system, several groups of fault detectors are installed on OTLs. The fault detectors (detection points) accurately acquire the transient current and detect the fault location. This system helps provide technical support for the proposed method. In this study, the reproduction method was implemented in 500-kV OTLs with the help of the distributed fault location system.

This paper is organized as follows. The analysis of a single phase-to-ground traveling wave is summarized in Sec. 2. In Sec. 3, the inversion theory and relative model are proposed. The fault reproduction method based on traveling waves is described in Sec. 4. In Sec. 5, various simulations were conducted to assess the performance of the proposed method, and the field application of the method is presented in Sec. 6. Concluding remarks are summarized in Sec. 7.

II. ANALYSIS OF A SINGLE PHASE-TO-GROUND FAULT TRAVELING WAVE

Fig. 1 illustrates the post-fault traveling wave process on OTLs. When a single phase-to-ground (A phase) fault occurs [as shown in Fig. 1(a)], the post-fault network [as shown in Fig. 1(b)] can be divided into a normal network and fault component network [as shown in Figs. 1(c) and 1(d)].

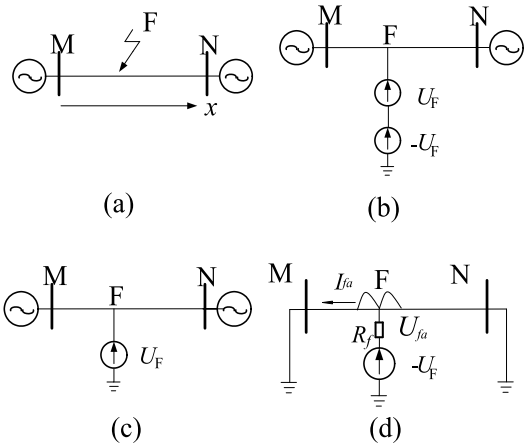

FIGURE 1. Fault traveling wave generation process for transmission lines. (a) SLG fault occurs in OTLs, (b) Post-fault network, (c) Normal network, (d) Fault component network.

In this paper, the Karenbauer transform [14] was adopted to decouple the three-phase current of OTLs. The phase amplitude transformation matrix $\mathbf{S}$ and inverse matrix $\mathbf{S}^{-1}$ are simplified as

$$\mathbf{S}=\begin{bmatrix}1 & 1 & 1\\ 1 & -2 & 1\\ 1 & 1 & -2\end{bmatrix},\quad \mathbf{S}^{-1}=\frac{1}{3}\begin{bmatrix}1 & 1 & 1\\ 1 & -1 & 0\\ 1 & 0 & -1\end{bmatrix}. \tag{1}$$

The initial traveling wave parameters are only related to the fault component network. The expression of the initial traveling wave at the fault point can be obtained as

$$I_0 = I_1 = I_2 = -\frac{U_F}{Z_0 + Z_1 + Z_2 + 6R_f} \tag{2}$$

where U_F is the A-phase voltage in the fault component network; R_f is the fault resistance; I_0, I_1, and I_2 represent the model current at the fault points; and Z_0, Z_1, and Z_2 are the model wave impedances of the OTL.

Combined with the Karenbauer transformation matrix, the model refraction current traveling wave generated by aerial- and ground-mode waves can be deduced as shown in (3) and (4), respectively:

$$\begin{cases} I_{0z} = -\dfrac{Z_1 + Z_2}{Z_0 + Z_1 + Z_2 + 6R_f}\dfrac{U_{r1}}{Z_1} \\ I_{1z} = I_{2z} = \dfrac{Z_0 + 6R_f}{Z_0 + Z_1 + Z_2 + 6R_f}\dfrac{U_{r1}}{Z_1} \end{cases}, \tag{3}$$

$$\begin{cases} I_{0z} = \dfrac{Z_1 + Z_2 + 6R_f}{Z_0 + Z_1 + Z_2 + 6R_f}\dfrac{U_{r0}}{Z_0} \\ I_{1z} = I_{2z} = -\dfrac{1}{Z_0 + Z_1 + Z_2 + 6R_f}U_{r0} \end{cases}, \tag{4}$$

where U_{r0} and U_{r1} represent the ground- and aerial-mode incident wave, respectively, and I_{0z}, I_{1z}, and I_{2z} denote the model refraction current traveling waves.

III. TRAVELING WAVE INVERSION

A. WAVEFORM INVERSION THEORY

In this paper, inversion theory [15], [16] was used to acquire the fault transient waveforms at the fault point. Inversion is a method of obtaining nearly best estimates of parameters, and it has been adopted for geophysical surveys.

According to inversion theory, the objective function is established by the residuals of forward and observed data. In addition, the unknown parameter can be acquired, whereas the objective function value is minimum. M represents the model space and M_1 is the subspace of M. D denotes the data space and D_1 represents the subspace of D. F is the forward operator mapped from M_1 to D_1. $\mathbf{m}$ is a vector, which refers to an element of M_1, and each element of the vector $\mathbf{m}$ is a function of model parameter $\mathbf{x}$ ($\mathbf{x}$ refers to a vector). The observed data $\mathbf{d}_{\text{obs}}$ are expressed as an N-dimensional vector, which is the element of D_1. Forward computation is a method of mapping the elements from model space M to data space D by the forward operator F, which contributes to obtaining the element $\mathbf{d}_{\text{cal}}$ in the data space, where $\mathbf{d}_{\text{cal}}$ is the forward modeling data.

The mathematic forward model can be derived as:

$$F\mathbf{m} = \mathbf{d}_{cal} \tag{5}$$

Similarly, the inversion model can be represented as:

$$\mathbf{m} = F^{-1}\mathbf{d}_{\text{obs}} \tag{6}$$

Owing to the existe ntial error from the observed data $\mathbf{d}_{\text{obs}}$, the residuals of forward and observed data are expressed as

$$\Delta\mathbf{d} = \mathbf{d}_{obs}\mathbf{d}_{cal} \tag{7}$$

Thus, the unknown model parameter is inverted based on F^{-1} and $\mathbf{d}_{obs}$. According to (6), a search for the best estimator of the model parameters involves the existing problems of instability and uniqueness of the approximate solution. Thus, a small observation error leads to a large deviation from the approximate solution and the true value. This is termed as the ill-posed problem and is typically encountered in engineering mathematics.

The inversion method is aimed at establishing an objective function $Q(\mathbf{m})$ based on residuals $\Delta\mathbf{d}$ and calculating the model parameter $\mathbf{x}$ with the lowest value of $Q(\mathbf{m})$. For the purpose of solving the ill-posed problem, regularization theory [17]–[20] is used to convert the ill-posed problem to an approximate well-posed problem. Therefore, we select L2-norm as the space of the objective function for parameter inversion, and the function is defined as

$$Q(\mathbf{m}) = \|F\mathbf{m} - \mathbf{d}_{obs}\|^2 = \|\mathbf{d}_{cal} - \mathbf{d}_{obs}\|^2 = \Delta\mathbf{d} \cdot \Delta\mathbf{d}^* \tag{8}$$

B. INVERSION MODEL FOR OTLS

Assuming that the distributed parameter for OTLs is uniform, detection points 1 and 2 are installed on the same side of the fault point along OTLs. Whenever a failure occurs, the current traveling wave will propagate along the detection points 1 and 2; the mathematical relations between traveling waves can be derived as

$$\begin{cases} I_2^{(i)} = I_1^{(i)} H^{(i)} = I_1^{(i)} e^{-\lambda^{(i)} d} \\ \lambda^{(i)} = \sqrt{(R^{(i)} + j\omega L^{(i)})(G^{(i)} + j\omega C^{(i)})} \end{cases} \tag{9}$$

where i ($i = 0, 1, 2$) represents the mode-i component. I_1 and I_2 are the fault current traveling waves obtained by detection points 1 and 2, respectively. d refers to the distance between points 1 and 2, λ is a frequency-dependent parameter; and R, L, G, and C denote resistance, inductance, conductance, and capacitance per unit length, respectively.

The transfer function is defined as:

$$H = e^{-\lambda x} \tag{10}$$

Based on the inversion theory, R, L, G, and C are analogous to the model parameter subspace. $H(\mathbf{m}) = e^{-\lambda(\mathbf{m})d}$ is analogous to model space. I_k ($k = 1, 2$) refers to the observed data at each detection point. According to (6), the inversion model based on distributed parameters$R$, L, G, and C can be established. The objective function of the parameter inversion is obtained as follows:

$$Q(\mathbf{m}) = \|\mathbf{d}_{cal} - \mathbf{d}_{obs}\|^2 = \|I_1 \cdot H(\mathbf{m}) - I_2\|^2 \tag{11}$$

Since a fault traveling wave contains abundant frequency components, the components at different frequencies have different propagation characteristics along OTLs. Therefore, (11) needs to be modified. In this study, a wavelet transform [21] is used to process waveforms by frequency division, which contributes to decomposing the pulse signal into different frequency bands and to obtaining accurate representation of signals.

According to wavelet theory, the wave energy is defined as the quadratic sum of reconstructed signals at a single scale. Thus, (11) is modified as follows:

$$Q(\mathbf{m}) = \sum_{j=1}^{n-1} k(j) \|I_1 \cdot H(\mathbf{m}) - I_2\|^2 \tag{12}$$

where $k(j)$ is the weight coefficient of section (j) after the $(n-1)$-layer wavelet transform, which was determined by the frequency-band energy ratio of the waveform. We used a six-layer, cubic B-spline mother wavelet for wavelet analysis of the traveling wave signal.

According to (5) and (9), the inversion model is established based on the distributed parameters R, L, G, and C. Thus, the unknown waveforms at the fault point can be inverted according to the obtained parameters and the observed data at the detection point. The flowchart of the inversion technique is shown in Fig. 2.

The detailed process of the inversion method to obtain the transient waveform at the fault point are as follows:

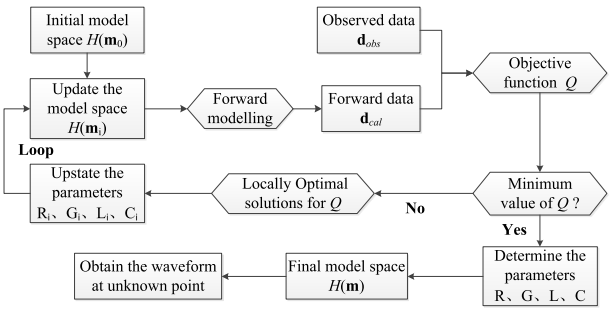

FIGURE 2. Flowchart of the inversion technique.

- Decouple the fault current traveling waves at the detection points 1 and 2 by using a Karenbauer transform.
- Utilize a six-layer wavelet transform to process the modulus components. A cubic B-spline mother wavelet is used to perform a wavelet analysis of the signals. Thus, waveforms in different frequency bands are obtained.
- Obtain the energy ratio $k(j)$ of different frequency bands. Subsequently, $k(j)$ is used as the weight coefficient of the objective function $Q(\mathbf{m})$.
- Process the decoupled wave data in different frequency bands by using fast Fourier transform where $I_{1(j)}^{(i)}$ and $I_{2(j)}^{(i)}$ represent the processed signals. The superscript i represents mode-i component. The subscript j represents the frequency-band number.

Thus, the objective function is obtained as follows:

$$\begin{cases} H_{(j)}^{(i)} = e^{-\lambda_{(j)}^{(i)} x}, \\ \lambda_{(j)}^{(i)} = \sqrt{(R^{(i)} + j \cdot 2\pi f_{(j)} L^{(i)})(G^{(i)} + j \cdot 2\pi f_{(j)} C^{(i)})} \\ Q(\mathbf{m}) = \sum_{j=1}^{n-1} k(j) \cdot (I_{1(j)}^{(i)} H_{(j)}^{(i)} - I_{1(j)}^{(i)}) \cdot (I_{1(j)}^{(i)} H_{(j)}^{(i)} - I_{1(j)}^{(i)})^* \end{cases} \quad (13)$$

where x denotes the propagation distance, and $f_{(j)}$ denotes the center frequency of different frequency bands.

- Obtain the unknown modulus distributed parameters $R^{(i)}$, $L^{(i)}$, $G^{(i)}$, and $C^{(i)}$. The distributed parameters is obtained by calculating the lowest value of the objective function $Q(\mathbf{m})$.
- Invert the fault traveling wave at the fault point. The transfer function $H_{(j)}^{(i)}$ is calculated after obtaining $R^{(i)}$, $L^{(i)}$, $G^{(i)}$, and $C^{(i)}$. The transient waveform at the fault point is inverted based on the inversion model of OTLs.

After obtaining the value of $H_{(j)}^{(i)}$, the wave data at the fault point is calculated as follows:

$$I_{f(j)}^{(i)} = I_{k(j)}^{(i)} / H_{(j)}^{(i)} \quad (14)$$

where $I_{f(j)}^{(i)}$ and $I_{k(j)}^{(i)}$ represent the signals at the fault point and the detection point, respectively.

As shown in (14), it is necessary to verify the uniqueness of the division operation to guarantee the uniqueness of the inversion result. $\lambda_{(j)}^{(i)}$ is expressed as:

$$\begin{cases} r = R^{(i)}, l = L^{(i)}, g = G^{(i)}, c = C^{(i)}, \omega = 2\pi f_{(j)} \\ \alpha = \sqrt{\frac{1}{2}\sqrt{(r^2 + \omega^2 l^2)(g^2 + \omega^2 c^2)} + \frac{1}{2}(rg - \omega^2 lg)} \\ \beta = \sqrt{\frac{1}{2}\sqrt{(r^2 + \omega^2 l^2)(g^2 + \omega^2 c^2)} - \frac{1}{2}(rg - \omega^2 lg)} \\ \lambda_{(j)}^{(i)} = \beta + j\alpha \end{cases} \quad (15)$$

Based on the distributed parameters and the center frequency, α and β correspond to deterministic values in each frequency band. Thus, the transfer function is expressed as follows:

$$H_{(j)}^{(i)} = e^{-\beta x} \cdot [\cos(-\alpha x) + j \sin(-\alpha x)] = c + jd \quad (16)$$

where c and d denote real numbers. Given that $I_{k(j)}^{(i)}$ is processed by a fast Fourier transform, it is expressed as $a + bj$. Therefore, $I_{f(j)}^{(i)}$ is expressed as $(a + jb)/(c + jd) = e + jf$, and the uniqueness of the inversion result is verified.

Also, the inverted and the actual waveforms are compared at other detection points (with the exception of points 1 and 2) to verify the accuracy of the inverted parameters and viability of the inversion method.

IV. FAULT REPRODUCTION MODEL AND Relevant Resolution Method

A. FAULT REPRODUCTION MODEL BASED ON WAVE INVERSION AND PROPAGATION CHARACTERISTICS

Fig. 3 shows the propagation process of traveling waves on OTLs, where M and N represent the bus at each terminal of the OTLs. f is the fault point and z and m are the detection points. Reflection and refraction will occur when the traveling wave encounters the special point (M, N, and f) due to its discontinuous surge impedance.

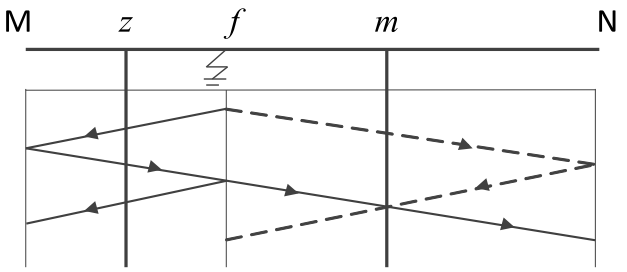

FIGURE 3. Propagation process of traveling wave.

The fault reproduction model is shown in Fig. 4, and the direction MN is stipulated to be a positive direction. m_1 and m_2, collectively called set m, represent the detection points installed on the positive direction side of point f. z_1 and z_2, collectively called set z, represent the detection points installed on the negative direction side of point f. M and N represent the bus. d_m and d_z denote the distance between each point in sets m and z, respectively. There are three situations according to fault location:

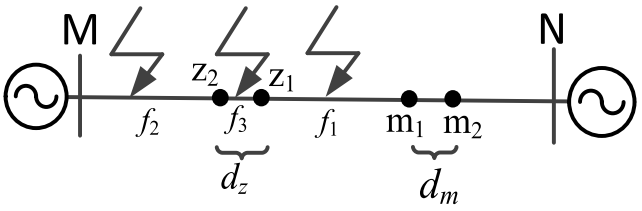

FIGURE 4. Model of fault reproduction.

- Between set z and m.
- On the same side of set z or m.
- Inside set z or m.

The three proposed situations are analyzed concretely below.

1) FAULTS OCCURING BETWEEN SET z AND m

$d_{z\mathrm{M}}$ is the distance between bus M and z_2, d_{mf1}, and d_{zf1} are the distance between f_1, m_1, and z_1, respectively. $d_{m\mathrm{N}}$ is the distance between bus N and m_1.

According to the first wavefront of the aerial-mode current traveling wave collected from set m, the initial traveling wave (positive direction) at the fault point can be obtained using the inversion method and its amplitude is written as I_{M}. Based on (2), I_{M} is defined as

$$I_M = -\frac{U_F}{Z_0 + Z_1 + Z_2 + 6R_f} \tag{17}$$

The aerial-mode wave velocity is greater than that of the ground mode. Therefore, when the second wavefront of the traveling wave detected by set m was analyzed, the wave component generated by the initial ground-mode traveling wave component was not considered in this paper. The second wavefront of the aerial-mode traveling wave detected by set m may be caused by the following two conditions:

- Condition 1: The initial wave at the fault point reaches bus M. Then, the wave reflected by bus M arrives at the fault point. Finally, the wave refracted by the fault point propagates to set m.
- Condition 2: The initial wave at the fault point reaches bus N. Then, the wave reflected by bus N propagates to set m.

Assuming that $d_{m\mathrm{N}} > d_{z\mathrm{M}} + 2d_z + d_{zf1}$. Referring to Fig. 3, the second wavefront is caused by condition 1. Therefore, according to the waveforms detected by set m, the secondary aerial-mode current traveling wave, which is generated by the initial wave at the fault point, reflected by bus M, and refracted by the fault point, could be obtained by an inversion calculation. I_m represents the amplitude of the secondary wave at the fault point.

Since the distance relation meets the requirement of the following inequality, $d_{m\mathrm{N}} > d_{z\mathrm{M}} + 2d_z + d_{zf1}$, the relation between $d_{\mathrm{M}z}$, d_{mf1}, d_m, and $d_{m\mathrm{N}}$ is derived as $d_{\mathrm{M}z} < d_{mf1} + d_m + d_{m\mathrm{N}}$. Based on the second wavefront detected by set z, the secondary aerial-mode current traveling wave, which is generated by the initial wave at the fault point, reflected by bus M, and propagated to the fault point before refraction, can be obtained by forward calculation. I_z represents the amplitude of the forward wave. Combining with (2) and (3), the ratio of I_m and I_z is derived as

$$\frac{I_m}{I_z} = \frac{Z_0 + 6R_f}{Z_0 + Z_1 + Z_2 + 6R_f} \tag{18}$$

If the distance relation meets the following inequality, $d_{m\mathrm{N}} < d_{z\mathrm{M}} + d_z + d_{zf1}$, the location of set mz could be exchanged equivalently, and the analytical procedure is the same as previously described. As U_F is only determined by line voltage and fault angle, the objective function can be established. Then, the value of the fault resistance and fault angle can be determined, which helps reproduce the process of the fault traveling wave and provides a quantitative analysis of fault information.

From the prior analysis, it can be seen that I_z is obtained by the inversion method based on the data collected from set z, so the reflection coefficient of bus M and the attenuation coefficient of traveling wave propagation are not considered in the proposed method. The objective function of the fault reproduction model is constructed as follows:

$$Q_{goal} = \sum_{i=1}^{2} \left\{ \begin{array}{l} \left\| \left| \frac{I'_{mi}}{I'_{zi}} \right| - \left| \frac{Z_0 + 6R_f}{Z_0 + Z_1 + Z_2 + 6R_f} \right| \right\|^2 \\ + \left\| \left| I'_{Mi} \right| - \left| \frac{U \sin\varphi}{Z_0 + Z_1 + Z_2 + 6R_f} \right| \right\|^2 \end{array} \right\} \tag{19}$$

where i refers to the modulus label, I'_{Mi} represents the amplitude of the aerial-mode current traveling wave inverted by the first wavefront (detected from set m), I'_{mi} represents the amplitude of the aerial-mode current traveling wave inverted by the second wavefront (detected from set m), and I'_{zi} represents the amplitude of the aerial-mode current traveling wave forwarded by the first wavefront (detected from set z). Z_0, Z_1, and Z_2 are the modulus wave impedances calculated by distribution parameters (the parameters are obtained using inversion method). U is the phase voltage amplitude on OTLs, φ is the fault initial angle, and R_f is the fault resistance.

2) FAULTS OCCURING ON THE SAME SIDE OF SET z AND m

Assuming that the fault location is between point z_1 and bus M, d_{zf2} is the distance between z_2 and fault point f_2, $d_{z\mathrm{N}}$ is the distance between z_1 and bus N, and $d_{\mathrm{M}f2}$ is the distance between fault point f_2 and bus M.

On the condition that $d_{\mathrm{M}f2} < d_{z\mathrm{N}}$, the data detected by set m are not necessarily considered. Based on the first wavefront detected by set z, the initial wave could be obtained using the inversion method (positive direction). The amplitude of the initial waveform is written as I_G, and the expression is the same as (17). According to the second wavefront detected by set z and inversion theory, the secondary aerial-mode traveling wave, which is generated by the initial wave at the fault point, reflected by bus M, and refracted by the fault point, can be obtained, and its amplitude is written as I_g.

The relation between I_G and I_g can then be derived as

$$\frac{I_g}{I_G} = \frac{e^{-2\alpha l}\beta_m(Z_0 + 6R_f)}{Z_0 + Z_1 + Z_2 + 6R_f} \tag{20}$$

where $l = d_{Mf2}$, α is the attenuation coefficient of the traveling wave, the value of α is the real part of $\sqrt{(R_1 + j\omega L_1)(G_1 + j\omega C_1)}$ (R_1, L_1, G_1, and C_1 represent distributed parameters), and β_m is the reflection coefficient of bus M.

In addition, if the fault occurs between bus N and detection point m_2, the distance relation is $d_{Mf2} > d_{zN}$. The locations of sets m and z could be exchanged equivalently. The analytical procedure is the same as that proposed above. The objective function of the fault reproduction model is constructed as follows:

$$Q_{goal} = \sum_{i=1}^{2} \left\{ \begin{array}{l} \left\| \left|\frac{I'_{gi}}{I'_{Gi}}\right| - \left| \frac{e^{-2\alpha l}\beta_m(Z_0 + 6R_f)}{Z_0 + Z_1 + Z_2 + 6R_f} \right| \right\|^2 \\ + \left\| |I'_{Gi}| - \left| \frac{U \sin\varphi}{Z_0 + Z_1 + Z_2 + 6R_f} \right| \right\|^2 \end{array} \right\} \tag{21}$$

where I'_{Gi} represents the amplitude of the aerial-mode current traveling wave inverted by the first wavefront (detected from point set z) and I'_{gi} represents the amplitude of the aerial-mode current traveling wave inverted by the second wavefront (detected from set z).

3) FAULTS OCCURING INSIDE SET z OR m

If the fault location is between z_1 and z_2, only the waveforms detected by points m_1 and m_2 are analyzed. d_{mN} is the distance between m_2 and bus N and d_{Mf3} denotes the distance between fault point f_3 and bus M.

Assuming that $d_{Mf3} < d_{mN}$, the initial aerial-mode traveling wave could be inverted by the first wavefront (obtained from detection points m_1 and m_2). In addition, the aerial-mode traveling wave, which is generated by the initial aerial-mode current traveling wave at the fault point, reflected by bus M, and refracted by the fault point, can be inverted by the second wavefront according to detection points m_1 and m_2. The method of establishing the objective function is the same as that proposed in Sec. 2). Furthermore, if the fault occurs between m_1 and m_2 (the distance relation is written as $d_{Mf3} > d_{mN}$), the location of sets m and z can be exchanged similarly.

B. CHAOS PARTICLE SWARM OPTIMIZATION ALGORITHM

In order to solve the objective function Q_{goal} of the proposed fault reproduction model, a specific algorithm should be adopted. PSO algorithm [22] is a new evolutionary algorithm developed in recent years. The PSO algorithm finds the global optimal solution by following the optimal value that is currently searched. The algorithm is advantageous for solving practical problems because of its ease of use, high precision, and fast convergence. However, when optimizing the objective function, the problem of a local optimum may occur. In order to improve the calculation accuracy, we combined a chaos algorithm with the PSO algorithm.

In this paper, the CPSO algorithm was adopted to apply an optimized solution for objective function Q_{goal}. PSO algorithm searches for an optimal solution through cooperation between individuals, and each particle discovers the optimal value of its own and the group to update its velocity and position in the process of iteration. The revised formula is written as

$$v_{k+1} = wv_k + c_1 n_1(p_{best,k} - x_k) + c_2 n_2(g_{best,k} - x_k) \tag{22}$$

$$x_{k+1} = x_k + v_{k+1} \tag{23}$$

where v_k represents the velocity vector of particle, x_k is the position of the current particle, $p_{best,k}$ is the position according to the individual optimal solution, $g_{best,k}$ is the position according to the global optimal solution, n_1 and n_2 are pseudorandom numbers ranging from 0 to 1, w is the inertial weight, and c_1 and c_2 are acceleration constants.

Since the chaotic motion has the properties of randomicity, ergodicity, etc., a chaos method could be used in the optimization process. When the particles appear to prematurely converge, chaotic disturbance enhances the efficiency of searching for an optimal solution, which helps increase the resulting precision and accelerate the convergence. Logistical mapping is selected to produce chaotic variables in this paper:

$$r_{j,k+1} = \mu r_{j,k}(1 - r_{j,k}) \tag{24}$$

where k is the number of iterations ($k = 0, 1, 2, \ldots, n$), j is the dimension, $r_{j,k}$ is the chaos parameter ($0 \leq r_{j,0} \leq 1$), and μ is a control parameter. When the parameter $\mu = 4$ and the parameter $r_0 \notin \{0, 0.25, 0.5, 0.75\}$, the logistics is completely in the chaotic state:

$$x_j = x_j^* + \lambda_j r_{j,k} \tag{25}$$

where x_j^* is the optimal solution based on current circumstances, λ_j is an adjustment coefficient, and $r_{j,k}$ is a chaotic variable ranging from -1 to 1.

As the search progresses from its start location, the variable gets closer to the optimal value, and accordingly the value of λ_j should gradually decrease. Thus, the value of λ_j is adjusted adaptively as follows:

$$\lambda_j = x_j^* \beta (1 - \frac{n_{now} - 2}{n_{\max}})^2 \tag{26}$$

where x_j^* is an optimal solution based on current circumstances, β is the radius of the neighborhood ($\beta = 0.15$), $n_{\max}$ denotes the maximum number of iterations, and n_{now} denotes the current number of iterations.

The entire process of the fault reproduction method is illustrated in Fig.5.

V. SIMULATIONS VERIFICATION OF THE PROPOSED METHOD

In order to evaluate the proposed fault reproduction method, we used PSCAD/EMTDC (Power Systems Computer Aided

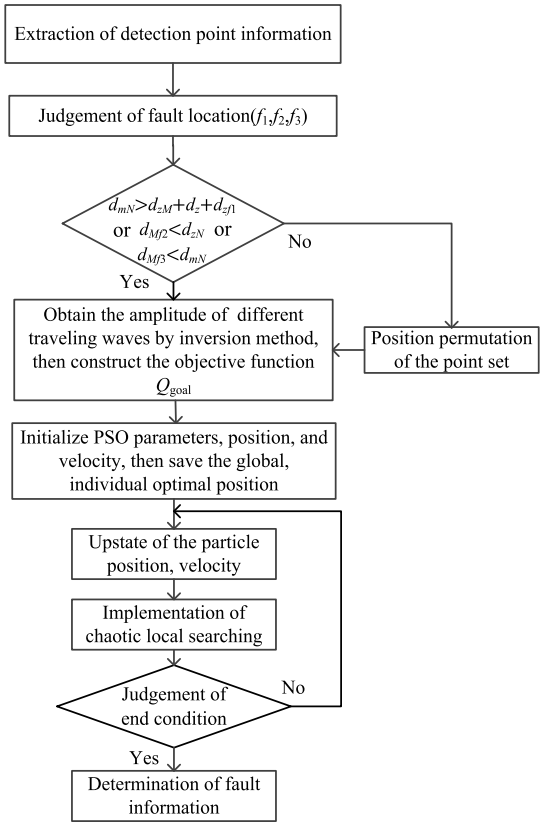

FIGURE 5. Process of fault reproduction method.

Design/ Electromagnetic Transients including DC)to carry out the fault reproduction simulations according to Fig. 4. The test case was a 400-km-long, 50-Hz transmission system. Four detectors were installed at points z_1, z_2, m_1, and m_2. The distance between m_2 and bus N was 250 km and the distance between z_2 and bus M was 80 km. $d_z = 15$ km and $d_m = 20$ km. A ZB1-type tower was used for the simulation. The magnitude of the detected voltage on the OTL was 350 kV and the sampling frequency was considered to be 1 MHz. A single phase-to-ground fault was studied in this system and the fault duration was 0.1 s. The reflection coefficient of bus M was set as 0.84. Simulation studies were carried out for various fault conditions, including different fault resistances and fault angles, to verify the feasibility of proposed method.

A. PROCESS OF PROPOSED METHOD

The distance between the fault point and bus M was 120 km. According to the distance relation, the fault position can be located between point set z and m ($d_{m\mathrm{N}} > d_{z\mathrm{M}} + d_z + d_{zf1}$).

The OTL distributed parameters obtained using the inversion method are presented in Table 1. Accordingly, the modulus wave impedance is calculated as follows: $Z_0 = 420.09\ \Omega$, $Z_1 = 150.76\ \Omega$, and $Z_2 = 150.75\ \Omega$. As the attenuation of traveling wave propagation has a more significant impact on zero-mode components, to improve the accuracy of the study the aerial-mode component was adopted for analysis.

TABLE 1. Values of distributed parameters for each modulus.

Mode	R(Ω/km)	G(S/km)	L(H/km)	C(F/km)
0	0.157459	0.097×10^{-7}	0.94977	0.5382×10^{-5}
1	0.018834	0.236×10^{-7}	0.158264	0.6963×10^{-5}
2	0.018709	0.207×10^{-7}	0.159077	0.6964×10^{-5}

TABLE 2. Wave information under different fault conditions obtained using the inversion method.

Fault angle (°)	Fault resistance (Ω)	I'_{m1} (A)	I'_{z1} (A)	I'_{M1} (A)	I'_{m2} (A)	I'_{z2} (A)	I'_{M2} (A)
30	0	111.79	190.07	241.86	112.22	189.09	240.17
	5	110.63	181.99	231.59	110.46	182.04	231.89
	10	109.04	129.72	223.32	109.01	175.82	223.63
	60	92.34	129.72	161.30	92.16	129.08	161.54
	250	54.32	64.34	78.79	54.56	63.94	79.12
60	0	193.64	329.18	418.82	194.36	325.33	413.25
	5	191.57	315.17	401.02	191.33	313.21	399.01
	10	188.85	304.55	386.75	187.55	302.47	384.82
	60	159.92	224.63	277.51	158.57	222.07	277.46
	250	94.03	111.39	135.56	93.86	110.10	136.18
90	0	222.13	375.64	483.56	223.01	375.52	484.25
	5	219.83	361.61	464.57	219.45	361.64	465.28
	10	217.69	349.38	450.22	217.85	349.29	450.94
	60	183.54	257.68	320.45	183.15	256.41	321.02
	250	107.97	127.80	156.61	108.43	127.19	157.31

I'_{m1} and I'_{m2}, amplitudes of mode-1 and mode-2 second wavefronts, respectively, inverted by point m_1. I'_{z1} and I'_{z2}, amplitudes of mode-1 and mode-2 second wavefronts, respectively, forwarded by point z_1. I'_{M1} and I'_{M2}, amplitudes of mode-1 and mode-2 first wavefronts, respectively, inverted by point m_1

Different amplitudes of the aerial-mode current traveling wave, which were obtained using the inversion method, are presented in Table 2. The case in which the fault angle is 90° and the fault resistance is 10 Ω was carried out for comparison's sake to prove the viability of the inversion method.

For example, the actual, inverted, or forwarded waveforms are presented in Figs. 6–8 with the following conditions: fault angle, 90°; fault resistance, 10 Ω. As shown in Fig. 6, the initial times of the actual and inverted mode-1 current traveling waves at detection point m_1 are 0.224906 and 0.224907 s, respectively. Therefore, the time deviation $t = 1\ \mu$s. The initial times of the real and inverted mode-2 current traveling waves at detection point m_1 are 0.224905 and 0.224906 s, respectively. The calculated time deviation $t = 1\ \mu$s. On the other hand, the amplitudes of the actual and inverted mode-1 waveforms are 448.1 and 450.2 Å, respectively, and the relative error is calculated as 0.47%. Similarly, the amplitudes of the actual and inverted mode-2 waveforms are 449.2 and 450.9 Å, respectively, and the relative error obtained is 0.38%. According to (9)–(10), we can infer that the inverted waveform at detection point m_1 is determined by distributed parameters and m_2 waveforms. Since the distributed parameters are uniform in this study, the inver-

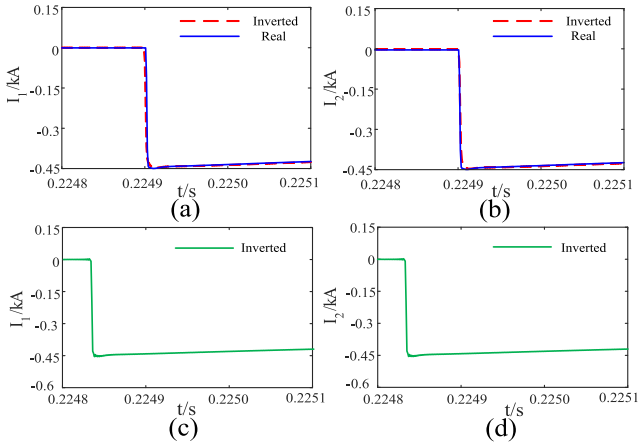

FIGURE 6. Waveforms obtained using the inversion method at m_1 (first wavefront). (a) mode-1 waveform at point m_1, (b) mode-2 waveform at point m_1, (c) mode-1 waveform at the fault point, (d) mode-2 waveform at the fault point.

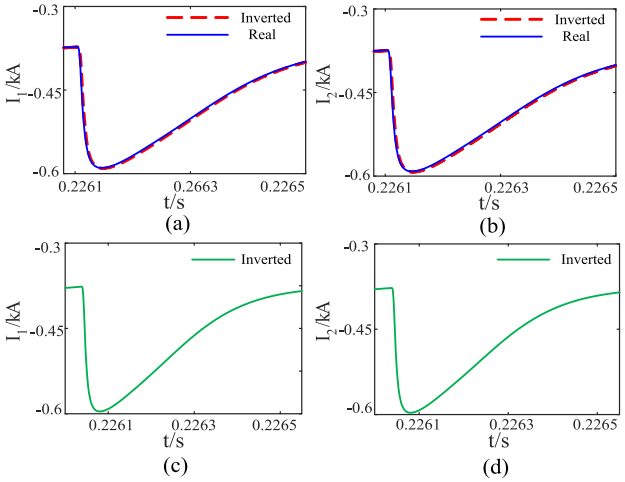

FIGURE 7. Waveforms obtained using the inversion method at m_1 (second wavefront). (a) mode-1 waveform at point m_1, (b) mode-2 waveform at point m_1, (c) mode-1 waveform at the fault point, (d) mode-2 waveform at the fault point.

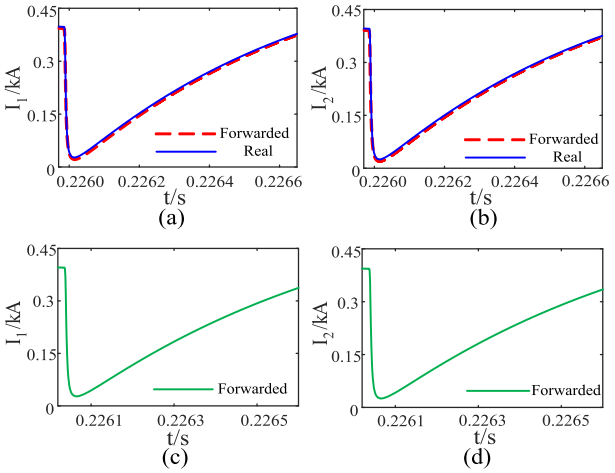

FIGURE 8. Waveforms obtained using inversion method at z_1 (second wavefront). (a) mode-1 waveform at point z_1, (b) mode-2 waveform at point z_1, (c) mode-1 waveform at the fault point, (d) mode-2 waveform at the fault point.

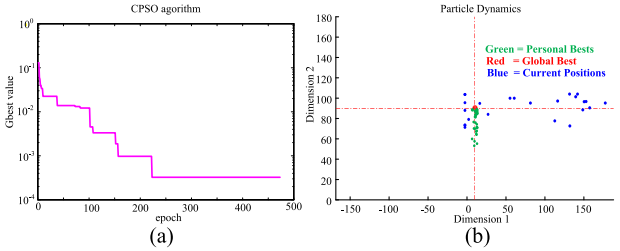

FIGURE 9. Operational process of CPSO algorithm.

sion accuracy at the fault point depends on the accuracy at point m_1. The calculated data above lead to the following conclusion: The inverted initial waveform and real waveform fit well and have high similarity. By analyzing the waveform data presented in Figs. 7 and 8, the maximum time deviation between the inverted (forwarded) and actual waveforms (second wavefront) can be obtained as 0.4 and 0.6 μs, respectively, and the maximum amplitude relative errors are 0.43% and 0.31%, respectively.

Fig. 9 presents the operational process of the CPSO algorithm (fault angle, 90°; fault resistance, 10 Ω). In order to reduce the uncertainty of the CPSO algorithm, the obtained fault information presented in Table 3 is the average of the results of 15 simulation runs.

The actual fault information in the simulation study is compared to the information obtained using fault reproduction method in Table 3. According to the fault information obtained from the proposed algorithm, the calculations are as follows: θ represents the maximum absolute error of fault angle and R refers to the maximum absolute error of fault resistance. The value of θ is 0.74°, whereas the actual fault angle is 60°. Moreover, the value of R is 2.67 Ω, whereas the actual fault resistance is 250 Ω, and the calculated relative error is only 1.07%.

B. COMPARISON BETWEEN DIFFERENT ALGORITHMS

In this study, the performance of the proposed optimization algorithm is analyzed. The CPSO algorithm is compared with the Simulated Annealing algorithm (SA), the Genetic algorithm (GA), the Ant Clony algorithm (AC) and the Artificial Fish Swarm algorithm (AFS) [23]–[26]. The fault angle is set as 30°, 45°, 60°, 90°, respectively. The fault angle is set as 0 Ω, 10 Ω, 100 Ω, 300 Ω, 500 Ω, respectively. Thus, the algorithms are tested under 20 different fault conditions. The averge and maximum error are obtained based on the actual and reproduced information. The comparison results of different algorithms are shown in Table 4.

When using the CPSO algorithm, the average error of the fault angle, the maximum error of the fault angle, the average error of the fault angle, and the maximum error of the fault angle are 0.25°, 0.76°, 0.54 Ω, and 2.35 Ω, respectively. It can be seen that the CPSO algorithm is slightly less effective

TABLE 3. Comparison of fault information.

Actual information		Reproduced information		Absolute error	
Fault angle (°)	Fault resistance (Ω)	Fault angle (°)	Fault resistance (Ω)	Fault angle (°)	Fault resistance (Ω)
30	0	30.04	0.02	0.04	0.02
30	5	30.00	4.89	0	0.11
30	10	29.34	10.03	0.66	0.03
30	60	30.00	60.63	0	0.63
30	250	29.76	252.18	0.24	2.18
60	0	60.13	0.09	0.13	0.09
60	5	60.23	4.90	0.23	0.1
60	10	59.69	10.16	0.31	0.16
60	60	59.26	60.11	0.74	0.11
60	250	60.17	248.12	0.17	1.88
90	0	90.06	0.03	0.06	0.03
90	5	90.00	4.99	0	0.01
90	10	89.24	10.00	0.76	0
90	60	89.58	59.83	0.42	0.17
90	250	90.19	252.67	0.19	2.67

TABLE 4. Comparison of different algorithms.

Algorithm	Fault angle (°)		Fault resistance (Ω)	
	Average error	Maximum error	Average error	Maximum error
PSO	0.47	0.84	0.86	3.66
CPSO	0.25	0.76	0.54	2.35
SA	0.67	0.93	1.19	4.55
GA	0.62	1.08	1.02	4.76
AC	0.45	0.87	0.79	2.75
AFS	0.51	0.95	0.98	2.33

than the AFS algorithm only for the maximum error of the fault resistance. With respect to other indices, the CPSO algorithm performs significantly better than other five algorithms. Thus, compared with other algorithms, the CPSO algorithm is more effective for reproducing the key information of a SPG fault.

C. ANALYSIS OF SIMULATION RESULTS

The inverted (or forwarded) waveforms are compared to real waveforms to verify the feasibility of the inversion method. According to the comparison, it has been proved that the inversion method can be adopted to obtain the OTL distributed parameters, the fault occurrence time, and the amplitude of the aerial-mode traveling wave accurately, which contributes to providing a theoretical basis for fault reproduction.

As seen from Table 3 and Table 4, the proposed algorithm can help to quantify the key information at the fault point with high accuracy. It can also be seen that fault conditions do not affect the performance of the proposed method.

VI. FIELD APPLICATION

The proposed method has been implemented in over 500 OTLs in China, including a double-circuit OTL with a length of 183.65 km. The arrangement of detection points is shown in Figs. 10(a) and 10(b). The magnitude of OTL voltage was 519.7 Kv, the sample rate 2 MHz, and the sample length 1200 μs. The detection points were installed at towers #34, #81, #130, and #167. The fault location system showed that the fault point was near F. Additional detection points were installed at towers #26, #59, #189, and #230. The distances from these additional points to bus M were 17.598, 30.143, 85.223, and 103.225 km, respectively.

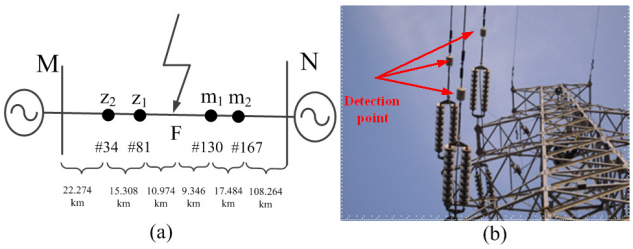

FIGURE 10. Arrangement of detection points in field application. (a) Diagram of the double-circuit OTL. (b) Diagram of the detection points installed on OTL.

On 12/19/2015 at 05:08:23 UTC, the traveling wave was captured successfully and the fault was identified as a single phase-to-ground fault. The power frequency component and the signal noise was removed. According to the distance relation and inversion theory, the required waveforms at detection points #130 and #81 were obtained.

The required mode-1 amplitudes of the inverted (or forwarded) waveform are 594.7, 258.1, and 422.2 Å, respectively, while the mode-2 amplitudes of the waveform are 597.9, 257.3, and 418.6 Å, respectively, for the points #130 and #81 mentioned above. On the basis of proposed fault reproduction method, the obtained key fault information is as follows: fault angle, 93.01°; fault resistance, 13.85 Ω; fault occurrence time, 26.3 μs. To verify the accuracy of the fault information, the additional points substituted for initial points equivalently. Similarly, by making use of the proposed fault reproduction method, the key fault information was obtained as follows: fault angle, 92.94°; fault resistance, 14.26 Ω; fault occurrence time, 26.2 μs. It was observed that there was little error compared to the previous case.

On the other hand, utility workers found a broken shield wire near F. As shown in Fig. 11(a), one terminal of the broken shield wire drooped to the ground. The location of the fault recording was near bus M, which was 48.56 km from F. The length of the drooping wire was 19 km, whereas the electrical resistivity of the conductor was 0.7 Ω/km. Therefore, the estimated value of the fault resistance was calculated as 13.3 Ω, which was identical to the result obtained by the proposed method. In addition, the results of the fault recording are presented in Fig. 11(b), and the fault angle was approximately 95.3°. Based on the fault recording informa-

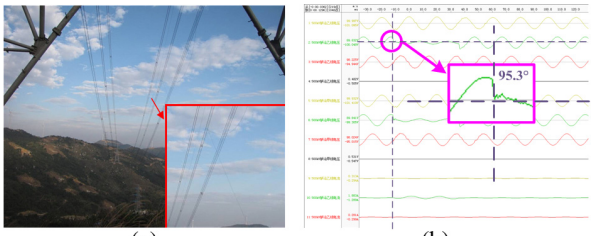

FIGURE 11. (a) Diagram of the broken shield wire. (b) Results of the fault recording.

tion and the location of the wave recording device, the fault angle at F can be estimated as 92.85°. It can be inferred that the reproduced information was consistent with the actual results. Thus, the accuracy and feasibility of the proposed method were proved, and the results of the fault reproduction are deemed applicable for line protection and fault analysis.

VII. CONCLUSION

Aimed at visualizing fault progress and acquiring key fault information, this paper proposes a reproduction method for SPG faults in OTLs. The inversion model is established on the basis of an OTL model, which helps obtain the distributed parameters and the transient traveling wave at the fault point. According to the simulation results, the inversion technique contributed to the acquisition of the transient waveforms at the fault point effectively. The experimental results demonstrate that the inverted waveforms have a high imitation degree compared to real waveforms. In addition, the proposed algorithm is able to execute a chaotic-local-search strategy in the calculation process, which is considered to have strong robustness. The comparison of fault information showed that the method had been proven to be feasible and accurate. The proposed fault reproduction method can also be adopted for other asymmetrical fault types, such as phase-to-phase and phase-to-phase-to-ground faults. Moreover, the proposed method has been implemented in over 500 OTLs in China, which has helped supply key information for fault analysis.

REFERENCES

[1] P. N. Bychkov, I. K. Zabrodina, and V. S. Shlapak, "Insulation contamination of overhead transmission lines by extreme service conditions," *IEEE Trans. Dielectr. Electr. Insul.*, vol. 23, no. 1, pp. 288–293, Feb. 2016.
[2] R. Billinton and J. R. Acharya, "Weather-based distribution system reliability evaluation," *IEE Proc.-Generat., Transmiss. Distrib.*, vol. 153, no. 5, pp. 499–506, Sep. 2006.
[3] D. Huang, J. Ruan, W. Cai, T. Li, Y. Wei, and J. Liu, "Flashover prevention on high-altitude HVAC transmission line insulator strings," *IEEE Trans. Dielectr. Electr. Insul.*, vol. 16, no. 1, pp. 88–98, Feb. 2009.
[4] X. Dong *et al.*, "Implementation and application of practical traveling-wave-based directional protection in UHV transmission lines," *IEEE Trans. Power Del.*, vol. 31, no. 1, pp. 294–302, Feb. 2016.
[5] W. C. Santos, F. V. Lopes, N. S. D. Brito, and B. A. Souza, "High-impedance fault identification on distribution networks," *IEEE Trans. Power Del.*, vol. 32, no. 1, pp. 23–32, Feb. 2017.
[6] T. Tsuboi, J. Takami, S. Okabe, K. Aoki, and Y. Yamagata, "Study on a field data of secondary arc extinction time for large-sized transmission lines," *IEEE Trans. Dielectr. Electr. Insul.*, vol. 20, no. 6, pp. 2277–2286, Dec. 2013.
[7] Y. Long, C. Yao, Y. Mi, D. Hu, N. Yang, and Y. Liao, "Identification of direct lightning strike faults based on mahalanobis distance and S-transform," *IEEE Trans. Dielectr. Electr. Insul.*, vol. 22, no. 4, pp. 2019–2030, Aug. 2015.
[8] C. Yao *et al.*, "A novel lightning current monitoring system based on the differential-integral loop," *IEEE Trans. Dielectr. Electr. Insul.*, vol. 20, no. 4, pp. 1247–1255, Aug. 2013.
[9] B. Rathore and A. G. Shaik, "Wavelet-alienation based transmission line protection scheme," *IET Generat., Transmiss. Distrib.*, vol. 11, no. 4, pp. 995–1003, 2017.
[10] F. V. Lopes, K. M. Silva, F. B. Costa, W. L. A. Neves, and D. Fernandes, "Real-time traveling-wave-based fault location using two-terminal unsynchronized data," *IEEE Trans. Power Del.*, vol. 30, no. 3, pp. 1067–1076, Jun. 2015.
[11] Y. Liu *et al.*, "Identification of lightning strike on 500-kV transmission line based on the time-domain parameters of a traveling wave," *IEEE Access*, vol. 4, pp. 7241–7250, 2016.
[12] Y. Long, C. Yao, Y. Mi, J. Wang, X. Tang, and R. Liao, "Preliminary full-waveform inversion of lightning current using differential-integral loop measurement," *IEEE Trans. Dielectr. Electr. Insul.*, vol. 23, no. 3, pp. 1534–1545, Jun. 2016.
[13] H. C. Shu, G. B. Zhang, and Z. Z. Zhu, "Inversion and restoration of lightning current waveform for shielding failure in 800 kV UHVDC transmission lines," (in Chinese), *J. Electr. Power Sci. Technol.*, vol. 29, no. 2, pp. 3–14, 2014.
[14] J. R. Ernst, H. Maurer, A. G. Green, and K. Holliger, "Full-waveform inversion of crosshole radar data based on 2-D finite-difference time-domain solutions of Maxwell's equations," *IEEE Trans. Geosci. Remote Sens.*, vol. 45, no. 9, pp. 2807–2828, Sep. 2007.
[15] J. Rao, M. Ratassepp, and Z. Fan, "Guided wave tomography based on full waveform inversion," *IEEE Trans. Ultrason., Ferroelect., Freq. Control*, vol. 63, no. 5, pp. 737–745, May 2016.
[16] C. Yao *et al.*, "A novel method to locate a fault of transmission lines by shielding failure," *IEEE Trans. Dielectr. Electr. Insul.*, vol. 21, no. 4, pp. 1573–1583, Aug. 2014.
[17] S. O. Haykin, *Neural Networks and Learning Machines*, vol. 3. Upper Saddle River, NJ, USA: Pearson, 2009.
[18] M. S. Zhdanov, *Geophysical Inverse Theory and Regularization Problems*. Amsterdam, The Netherlands: Elsevier, 2002.
[19] Y. Wang, A. G. Yagola, and C. Yang, *Optimization and Regularization for Computational Inverse Problems and Applications*. Beijing, China: Higher Education Press, 2011.
[20] P. C. Hansen, *Rank-Deficient and Discrete Ill-Posed Problems: Numerical Aspects of Linear Inversion*. Philadelphia, PA, USA: SIAM, 1998.
[21] S. A. Saleh and M. A. Rahman, "Modeling and protection of a three-phase power transformer using wavelet packet transform," *IEEE Trans. Power Del.*, vol. 20, no. 2, pp. 1273–1282, Apr. 2005.
[22] J. Kennedy, "Particle swarm optimization," in *Encyclopedia of Machine Learning*, C. Sammut and G. I. Webb, Eds. New York, NY, USA: Springer, 2011, pp. 760–766.
[23] P. J. M. van Laarhoven and E. H. L. Aarts, "Simulated annealing," in *Simulated annealing: Theory and Applications*. Eindhoven, The Netherlands: Springer, 1987, pp. 7–15.
[24] K. Deb, A. Pratap, S. Agarwal, and T. Meyarivan, "A fast and elitist multiobjective genetic algorithm: NSGA-II," *IEEE Trans. Evol. Comput.*, vol. 6, no. 2, pp. 182–197, Apr. 2002.
[25] M. Dorigo, M. Birattari, and T. Stutzle, "Ant colony optimization," *IEEE Comput. Intell. Mag.*, vol. 1, no. 4, pp. 28–39, Nov. 2006.
[26] W. Shen, X. Guo, C. Wu, and D. Wu, "Forecasting stock indices using radial basis function neural networks optimized by artificial fish swarm algorithm," *Knowl.-Based Syst.*, vol. 24, no. 3, pp. 378–385, 2011.

HANQING LIANG was born in Beijing, China. He received the B.S. degree in electrical engineering from North China Electric Power University, Beijing, in 2015. He is currently pursuing the Ph.D. degree in electrical engineering with Shanghai Jiaotong University, Shanghai, China. His research interests include detecting fault location and the diagnosis of power equipment.

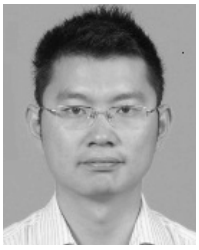

YADONG LIU (M'11) was born in Wuhan, China. He received the B.E. degree in electronic and information from the China University of Geosciences, Wuhan, in 2004, and the M.D. and Ph.D. degrees in electrical engineering from Shanghai Jiao Tong University (SJTU), Shanghai, China, in 2008 and 2012, respectively. He is currently a Lecturer with the School of Electronic Information and Electrical Engineering, SJTU. His research interests include detecting fault location and the diagnosis of power equipment.

GEHAO SHENG (M'08) was born in Hunan, China. He received the B.E. and Ph.D. degrees from the Huazhong University of Science and Technology, Wuhan, China, in 1996 and 2003, respectively. He is currently a Full Professor of electrical engineering with Shanghai Jiao Tong University, Shanghai, China. His research interests include control theory and its applications to automatic voltage control in power systems.

XIUCHEN JIANG was born in Shandong, China. He received the degree from Shanghai Jiao Tong University (SJTU), Shanghai, China, in 1987, the M.D. degree in electrical engineering from Tsinghua University, Beijing, China, in 1992, and the Ph.D. degree in electrical engineering from SJTU in 2001. He is currently a Full Professor with SJTU, where he has been acting as the Director of Electrical Power Department since 2002. His main research fields are in electrical measuring technology and electrical apparatus automation.